

# Wavelet-based Synchronization of Nongated Confocal Microscopy Data for 4D Imaging of the Embryonic Heart

*Invited Paper*

Michael Liebling<sup>1</sup>, Arian S. Forouhar<sup>2</sup>, Morteza Gharib<sup>2</sup>, Scott E. Fraser<sup>1</sup>, Mary E. Dickinson<sup>1,3</sup>

<sup>1</sup>Biological Imaging Center, Beckman Institute, California Institute of Technology,  
Mail Code 139-74, Pasadena, CA 91125, USA;

<sup>2</sup>Bioengineering Option, California Institute of Technology,  
Mail Code 205-45, Pasadena, CA 91125, USA;

<sup>3</sup>Department of Molecular Physiology and Biophysics, Baylor College of Medicine,  
One Baylor Plaza, Houston, TX 77030, USA.

## ABSTRACT

With the availability of new confocal laser scanning microscopes, fast biological processes, such as the blood flow in living organisms at early stages of the embryonic development, can be observed with unprecedented time resolution. When the object under study has a periodic motion, e.g. a beating embryonic heart, the imaging capabilities can be extended to retrieve 4D data. We acquire nongated slice-sequences at increasing depth and retrospectively synchronize them to build dynamic 3D volumes. Here, we present a synchronization procedure based on the temporal correlation of wavelet features. The method is designed to handle large data sets and to minimize the influence of artifacts that are frequent in fluorescence imaging techniques such as bleaching, nonuniform contrast, and photon-related noise.

**Keywords:** Wavelets, confocal laser scanning microscopy, dynamic cardiac imaging, nongated synchronization.

## 1. INTRODUCTION

One of the most challenging objectives in developmental biology is being able to acquire, visualize, and analyze three-dimensional time-series (4D data) at high frame-rates. Dynamic *in vivo* imaging of fast biological processes at the cellular and sub-cellular levels requires appropriate microscopes and procedures. While the 1–2 frames per second (fps) frame-rate of a conventional confocal microscope is sufficient to monitor slow movements (e.g. cell migrations occurring at 20–50  $\mu\text{m}/\text{h}$ , see Ref.<sup>1</sup>), the swifter ones (e.g. red blood cells in the developing cardio-vascular system, that move at 1–10 mm/s, see Ref.<sup>2</sup>), or those imaged at high magnification, require 1 to 2 orders of magnitude faster microscopes. Imaging the developing heart in the zebrafish embryo typically requires acquisition speeds of 100 fps and above.

Recent developments in fast confocal laser scanning microscopy (such as those implemented in the Zeiss LSM 5 LIVE<sup>3</sup> microscope) allow the acquisition of 2D slices at high frame-rates, i.e. above 120 frames per second (fps). Direct dynamic 3D imaging is currently not possible without reducing the acquisition rate by at least one order of magnitude. This makes the observation and analysis of the fast-moving heart-wall cells difficult. Indeed, it is not possible to gain insights into the 3D geometry from 2D slice-sequences only and too low a frame rate induces aliasing and blurring artifacts.

Despite this limitation, and when the imaged motion is periodic, it is possible to reconstruct dynamic 3D volumes from sequentially acquired 2D slice-sequences (at different positions along the  $z$ -axis of the sample) without giving up temporal resolution. Similar approaches are commonly used for cardiac imaging using other, macroscopic, modalities such as magnetic resonance imaging, computerized tomography, or ultrasound<sup>4–11</sup>; if the acquisition is always triggered at the same moment in the heart cycle (gated acquisition), the different slice-sequences can directly be assembled to form a dynamic 3D volume. In the absence of a reliable external gating signal, the acquisition intervals do not match (nongated acquisition) and direct reconstruction is not possible. In the case of the beating embryonic zebrafish heart, it is currently difficult to acquire a reliable external gating signal, implying that the sequences are nongated. In order to synchronize them a posteriori (post-acquisition synchronization), we have developed a procedure based exclusively on the information

---

M.L.: E-mail: liebling@caltech.edu, Telephone: 626-395-2863.

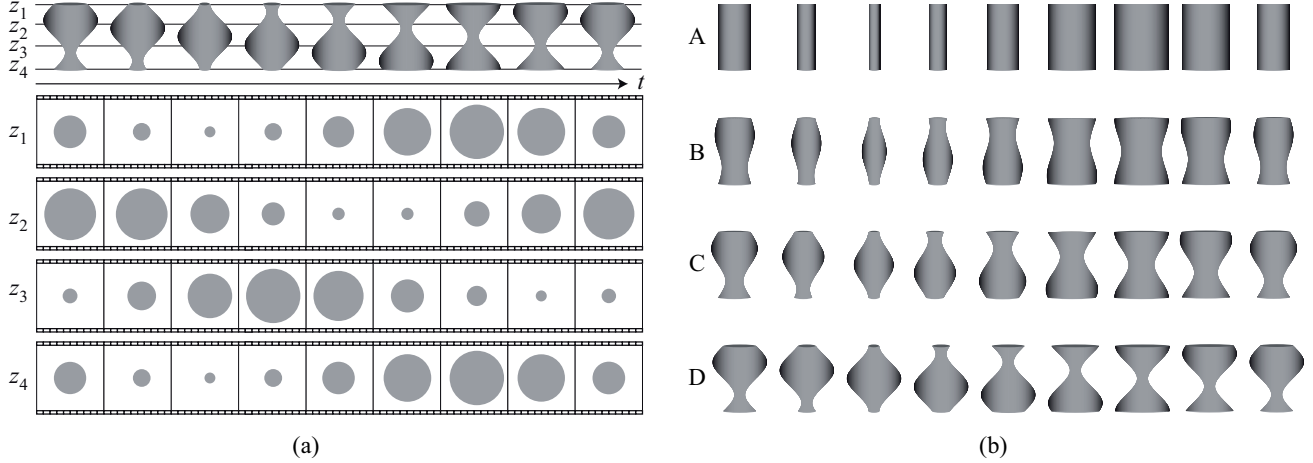


**Figure 1.** Consistent reconstruction is not possible if the acquisition procedure is not compatible with the imaged motion. (a) Time-sequence of a periodically constricting tube and measured slice-sequences (ideal PSF) (b) Time-sequences of four different objects that yield equivalent measurements (up to a temporal shift). From the measurements in (a) the least-squares criterion yields the 3D object depicted in A.

contained in the nongated sequences themselves.<sup>12</sup> Because of the tremendous amount of data involved for 4D imaging and the specificity of fluorescence imaging artifacts, the alignment is carried out on a limited set of thresholded wavelet coefficients corresponding to specific frequency-bands. Here, we review and further discuss some characteristics of this method.

## 2. ALGORITHM

During acquisition, the measured intensity is given by

$$I_m(\mathbf{x}, z_k, t) = \iiint I(\mathbf{x}', z, t - s_k) \text{PSF}(\mathbf{x} - \mathbf{x}', z - z_k) d\mathbf{x}' dz \quad (1)$$

with  $s_k$  the unknown time shift at depth  $z_k = kh$ ,  $k = 0, \dots, N_z$ , where  $h$  is the axial slice spacing. The optical system's point spread function is denoted PSF. We assume that the measured intensity is periodic with period  $T$ , i.e.,

$$|I(\mathbf{x}, z, t) - I(\mathbf{x}, z, t + T)| \ll I_{\max}, \quad (2)$$

and that each sequence has a duration  $L = mT$  with  $m \in \mathbb{N}^*$ . In order to recover the original volume  $I(\mathbf{x}, z, t)$  from the measurements  $I_m(\mathbf{x}, z_k, t)$ , we consider the following objective least-squares criterion to measure the similarity between the data from neighboring depths  $z_k$  and  $z_{k'}$

$$\begin{aligned} Q_{k,k'}(s) &= \iint_{\mathbb{R}^2} \int_0^L |I_m(\mathbf{x}, z_k, t)|^2 + |I_m(\mathbf{x}, z_{k'}, t - s)|^2 dt d\mathbf{x} \\ &= C - 2 \iint_{\mathbb{R}^2} \int_0^L I_m(\mathbf{x}, z_k, t) I_m(\mathbf{x}, z_{k'}, t - s) dt d\mathbf{x}, \end{aligned} \quad (3)$$

where  $C$  is a constant. The shift  $s \in \mathbb{R}$  that minimizes  $Q_{k,k'}(s)$  corresponds to the relative shift  $s_{k,k'}$  between two pairs of  $z$ -slices at depths  $z_k$  and  $z_{k'}$ . To achieve consistent reconstructions, the acquisition must be performed with a sampling step  $h$  in the  $z$ -direction that is smaller than the axial extent of the point spread function. In Fig. 1 (a), we show a deformation that is not homogeneous with respect to the  $z$ -direction, and is acquired with a device whose point spread function does not fulfill the latter requirement,

$$\text{PSF}(\mathbf{x}, z) = \delta(\mathbf{x})\delta(z). \quad (4)$$

In that case, the similarity criterion (3) yields an erroneous reconstruction, i.e. object A, depicted in Fig. 1 (b). Note that objects A–D all yield equivalent slice-sequences, up to a temporal shift. Accurate reconstructions are only possible if the axial PSF-extent is larger than the  $z$ -sampling step  $h$ , the motion is known a priori to be homogeneous in the  $z$ -direction, or supplementary information is available (electrocardiogram,...).

The quantity in Eq. (3) strongly depends on the image-sequence quality. The images are typically corrupted by noise, non-uniform background, etc. Therefore, instead of correlating image pixels (in time), we correlate wavelet coefficients. To this end, we consider a separable orthogonal wavelet basis of  $L_2(\mathbf{R}^2)$ ,

$$\{\psi_{j,\mathbf{m}}^1(\mathbf{x}), \psi_{j,\mathbf{m}}^2(\mathbf{x}), \psi_{j,\mathbf{m}}^3(\mathbf{x})\}_{j \in \mathbf{Z}, \mathbf{m} \in \mathbf{Z}^2} \quad (5)$$

where the two-dimensional wavelets

$$\psi_{j,\mathbf{m}}^p(\mathbf{x}) = \frac{1}{2^j} \psi^p\left(\frac{\mathbf{x}}{2^j} - \mathbf{m}\right) \quad (6)$$

are constructed with separable products of the 1D scaling function  $\phi(x)$  and wavelet  $\psi(x)$

$$\psi^1(\mathbf{x}) = \phi(x)\psi(y), \psi^2(\mathbf{x}) = \psi(x)\phi(y), \psi^3(\mathbf{x}) = \psi(x)\psi(y). \quad (7)$$

We index the basis functions with a single index  $\mathbf{k}$  that includes the scale  $j \in \mathbf{Z}$ , translation  $\mathbf{m} \in \mathbf{Z}^2$ , and wavelet type  $p \in \{1, 2, 3\}$ :

$$\psi_{\mathbf{k}}(\mathbf{x}) = \psi_{j,\mathbf{m}}^p(\mathbf{x}), \quad \mathbf{k} = (p, j, \mathbf{m}). \quad (8)$$

An image, at a fixed depth  $z_k$  and time-point  $t$ , is expanded in the wavelet basis as

$$I_m(\mathbf{x}, z_k, t) = \sum_{\mathbf{k}} c_{k,\mathbf{k}}(t) \psi_{\mathbf{k}}(\mathbf{x}) \quad (9)$$

where the coefficients are given by the inner products (wavelet transform)

$$c_{k,\mathbf{k}}(t) = \langle I_m(\cdot, z_k, t), \psi_{\mathbf{k}} \rangle \quad (10)$$

$$= \iint I_m(\mathbf{x}, z_k, t) \psi_{\mathbf{k}}(\mathbf{x}) \, d\mathbf{x}. \quad (11)$$

Since the basis functions are orthogonal, i.e.  $\langle \psi_{\mathbf{k}}, \psi_{\mathbf{k}'} \rangle = \delta_{\mathbf{k},\mathbf{k}'}$ , we may rewrite Eq. (3) as

$$\begin{aligned} Q_{k,k'}(jh_t) &= C - 2 \int_0^L \sum_{\mathbf{k}} c_{k,\mathbf{k}}(t) c_{k',\mathbf{k}}(t - jh_t) \, dt \\ &\approx C - 2h_t \sum_{\mathbf{k}} \sum_{i=0}^{N_t-1} c_{k,\mathbf{k}}(ih_t) c_{k',\mathbf{k}}[(i-j)h_t]. \end{aligned} \quad (12)$$

$\mathbf{k}$  spans a finite number of scales and translations since the image support as well as the initial image resolution are finite.

The number of wavelet coefficients is the same as the number of pixels [see Fig. 2 (b)]. Therefore, the evaluation of Eq. (12) has the same complexity as Eq. (3). However, since the wavelet transform is an organized and concise representation of the signal, it allows us to work with a subset of the full dataset. For our purposes, we may discard the higher frequency bands, an operation which results in a important data-size reduction. To avoid contributions to the correlation signal from non-uniform background artifacts (that may vary with time) we discard the low frequency coefficients [see Fig. 2 (c)]. Robustness to random photon noise is obtained via a soft-threshold of the remaining coefficients. Although Eq. (12) requires an orthogonal wavelet basis to be strictly valid, we implemented our algorithm with Daubechies 9/7 wavelets<sup>13</sup>: They are nearly orthogonal, have good approximation properties, and are symmetric.<sup>14</sup> The latter property allows for implementations that do not require that the image-size be a multiple of a power-of-two.<sup>15</sup> Therefore, it is also possible to perform the synchronization on manually selected regions-of-interest.

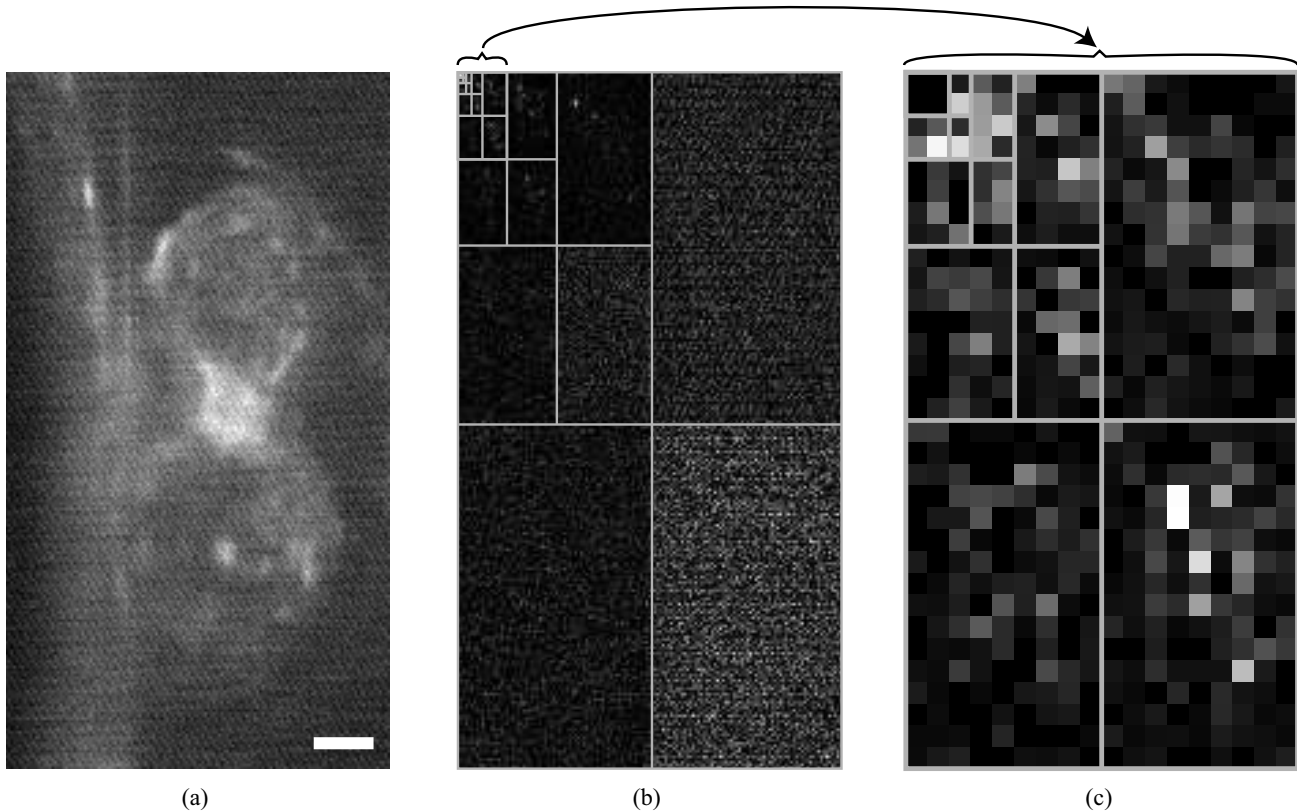


**Figure 2.** Data Reduction. (a) Raw-data frame of confocal slice through the embryonic heart,  $256 \times 141$  pixels. Scale-bar is  $20 \mu\text{m}$ . (b) Wavelet Transform,  $256 \times 141$  pixels. (c) The registration is performed on the reduced data-set obtained by cropping the lowest and the three highest frequency bands and applying a hard threshold to the remaining coefficients. The image is  $32 \times 18$  pixels.

### 3. RESULTS

In Fig. 2 (a), we show a single frame of a sequence acquired in a 48 hours post fertilization (hpf) transgenic zebrafish embryo<sup>16</sup> (*danio rerio*) using a prototype of the Zeiss LSM 5 *LIVE* microscope.<sup>3</sup> The zebrafish heart's two chambers, the atrium and the ventricle, are visible, separated by the atrioventricular canal (center). The image is corrupted by various artifacts, including structured noise, nonuniform background, detector and photon noise. Fig. 2 (b) shows the corresponding wavelet coefficients. In order to perform the time-synchronization in a robust manner, we only keep the four lowest frequency scales (since high frequency bands are corrupted by structured noise and we want to reduce the data size), and remove the lowest frequency band (to avoid dependence on a non-uniform background). We apply a soft threshold to the remaining coefficients. Compared to the original  $256 \times 141$  pixel large picture, the synchronization is based on the correlation of the  $32 \times 18$  wavelet coefficients, a reduction in size of about 70%. Finally, in Fig. 3, we show the rendering of data from a 54 hpf zebrafish heart. The atrium and ventricle have been segmented. Three-dimensional renderings allow for the precise inspection of the heart development.

### 4. CONCLUSION

Recently developed confocal microscopes allow imaging of fast processes with good depth discrimination. For periodic motions, 4D data may be reconstructed reliably from nongated slice-sequences by use of a wavelet-based synchronization method. The approach benefits from the concise data and selective space-frequency wavelet representations, and allows to overcome size constraints and acquisition artifacts. For some particular deformations, and when the sampling along the  $z$ -axis is too sparse compared to the axial point spread function extent, supplementary information is required to achieve correct reconstructions.

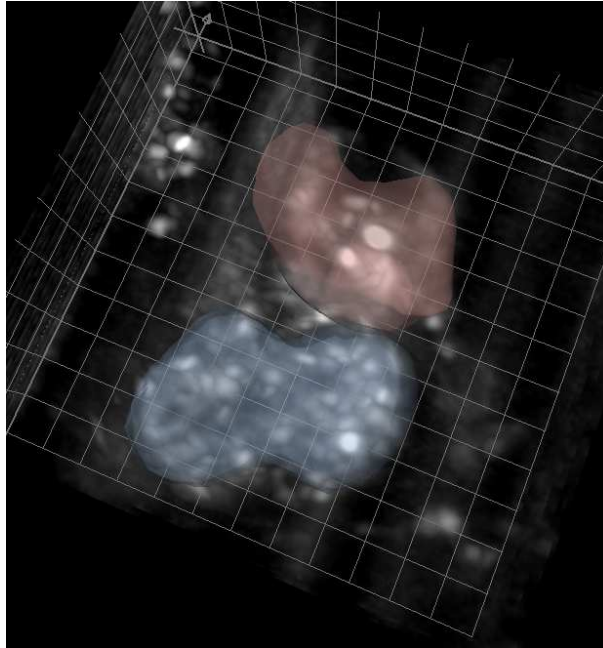


**Figure 3.** 3D reconstruction of a zebrafish heart. The atrium and ventricle have been segmented. The grid spacing is 20  $\mu\text{m}$ . (Rendering obtained using Imaris, Bitplane AG)

### ACKNOWLEDGMENTS

We thank S. Lin for the transgenic *gatal::GFP* zebrafish line. Michael Liebling was partially supported by a postdoc grant from the Swiss National Science Foundation no. PBEL2-104418.

### REFERENCES

1. Y.-T. Shiu, S. Li, W. A. Marganski, S. Usami, M. A. Schwartz, Y.-L. Wang, M. Dembo, and S. Chien, "Rho mediates the shear-enhancement of endothelial cell migration and traction force generation," *Biophys J* **86**, pp. 2558–2565, 2004.
2. E. A. V. Jones, M. H. Baron, S. E. Fraser, and M. E. Dickinson, "Measuring hemodynamic changes during mammalian development," *American Journal of Physiology—Heart and Circulatory Physiology* **287**, pp. H1561–H1569, Oct. 2004.
3. Carl Zeiss AG, "LSM 5 LIVE." <http://www.zeiss.de/>.
4. T. A. Spraggins, "Wireless retrospective gating—application to cine cardiac imaging," *Magnetic Resonance Imaging* **8**(6), pp. 675–681, 1990.
5. R. D. White, C. B. Paschal, M. E. Clampitt, T. A. Spraggins, and G. W. Lenz, "Electrocardiograph-independent, wireless cardiovascular cine MR imaging," *Journal of Magnetic Resonance Imaging* **1**, pp. 347–355, May–June 1991.
6. M. E. Crowe, A. C. Larson, Q. Zhang, J. Carr, R. D. White, D. B. Li, and O. P. Simonetti, "Automated rectilinear self-gated cardiac cine imaging," *Magnetic Resonance in Medicine* **52**, pp. 782–788, Oct. 2004.
7. A. C. Larson, R. D. White, G. Laub, E. R. McVeigh, D. B. Li, and O. P. Simonetti, "Self-gated cardiac cine MRI," *Magnetic Resonance in Medicine* **51**, pp. 93–102, Jan. 2004.
8. M. Grass, R. Manzke, T. Nielsen, P. Koken, R. Proksa, M. Natanzon, and G. Shechter, "Helical cardiac cone beam reconstruction using retrospective ECG gating," *Physics in Medicine and Biology* **48**, pp. 3069–3084, Sept. 2003.
9. M. Kachelrieß, D. A. Sennst, W. Maxlmoser, and W. A. Kalender, "Kymogram detection and kymogram-correlated image reconstruction from subsecond spiral computed tomography scans of the heart," *Medical Physics* **29**, pp. 1489–1503, July 2002.

10. G. M. Treece, R. W. Prager, A. H. Gee, C. J. C. Cash, and L. Berman, "Grey-scale gating for freehand 3D ultrasound," in *Proceedings of the First 2002 IEEE International Symposium on Biomedical Imaging: Macro to Nano (ISBI'02)*, pp. 993–996, (Washington DC, USA), July 7-10, 2002.
11. S. A. de Winter, R. Hamers, M. Degertekin, K. Tanabe, P. A. Lemos, P. W. Serruys, J. R. T. C. Roelandt, and N. Bruining, "Retrospective image-based gating of intracoronary ultrasound images for improved quantitative analysis: The intelligate method," *Catheterization and Cardiovascular Interventions* **61**, pp. 84–94, Jan. 2004.
12. M. Liebling, A. S. Forouhar, M. Gharib, S. E. Fraser, and M. E. Dickinson, "4-dimensional cardiac imaging in living embryos via post-acquisition synchronization of nongated slice-sequences," *J. Biomed. Opt.*, *in press*.
13. M. Antonini, M. Barlaud, M. Mathieu, and I. Daubechies, "Image coding using wavelet transform," *IEEE Trans. Image Proces.* **1**, pp. 205–220, Apr. 1992.
14. M. Unser and T. Blu, "Mathematical properties of the JPEG2000 wavelet filters," *IEEE Transactions on Image Processing* **12**, pp. 1080–1090, Sept. 2003.
15. C. M. Brislawn, "Classification of nonexpansive symmetric extension transforms for multirate filter banks," *Applied and Computational Harmonic Analysis* **3**, pp. 337–357, Oct. 1996.
16. Q. M. Long, A. M. Meng, H. Wang, J. R. Jessen, M. J. Farrell, and S. Lin, "GATA-1 expression pattern can be recapitulated in living transgenic zebrafish using GFP reporter gene," *Development* **124**, pp. 4105–4111, Oct. 1997.